

Differences in electrophysiological properties of functionally identified nociceptive sensory neurons in an animal model of cancer-induced bone pain

Yong Fang Zhu, PhD¹, Robert Ungard, MSc¹, Eric Seidlitz, PhD¹, Natalie Zacal, MSc¹, Jan Huizinga, PhD², James L Henry, PhD³ and Gurmit Singh, PhD¹

Molecular Pain
Volume 12: 1–14
© The Author(s) 2016
Reprints and permissions:
sagepub.co.uk/journalsPermissions.nav
DOI: 10.1177/1744806916628778
mpx.sagepub.com


Abstract

Background: Bone cancer pain is often severe, yet little is known about mechanisms generating this type of chronic pain. While previous studies have identified functional alterations in peripheral sensory neurons that correlate with bone tumours, none has provided direct evidence correlating behavioural nociceptive responses with properties of sensory neurons in an intact bone cancer model.

Results: In a rat model of prostate cancer-induced bone pain, we confirmed tactile hypersensitivity using the von Frey test. Subsequently, we recorded intracellularly from dorsal root ganglion neurons *in vivo* in anesthetized animals. Neurons remained connected to their peripheral receptive terminals and were classified on the basis of action potential properties, responses to dorsal root stimulation, and to mechanical stimulation of the respective peripheral receptive fields. Neurons included C-, A δ -, and A β -fibre nociceptors, identified by their expression of substance P. We suggest that bone tumour may induce phenotypic changes in peripheral nociceptors and that these could contribute to bone cancer pain.

Conclusions: This work represents a significant technical and conceptual advance in the study of peripheral nociceptor functions in the development of cancer-induced bone pain. This is the first study to report that changes in sensitivity and excitability of dorsal root ganglion primary afferents directly correspond to mechanical allodynia and hyperalgesia behaviours following prostate cancer cell injection into the femur of rats. Furthermore, our unique combination of techniques has allowed us to follow, in a single neuron, mechanical pain-related behaviours, electrophysiological changes in action potential properties, and dorsal root substance P expression. These data provide a more complete understanding of this unique pain state at the cellular level that may allow for future development of mechanism-based treatments for cancer-induced bone pain.

Keywords

Bone cancer, pain, primary afferent, dorsal root ganglion, electrophysiology, behaviour, prostate cancer

Date received: 19 November 2015; accepted: 4 December 2015

Background

Cancer-induced bone pain (CIBP) is a severe and often intractable type of cancer pain and is a significant contributor to patient morbidity and quality of life.^{1–5} Due to its often widespread distribution, patients with bone metastases remain faced with limited treatment options both for arresting the progression of the disease itself and for limiting pain. Until recently, there has been little basic scientific investigation aimed at understanding

¹Michael G. DeGroote Institute for Pain Research and Care, Department of Pathology and Molecular Medicine, McMaster University, Hamilton, Ontario, Canada

²Farncombe Family Digestive Health Research Institute, Department of Medicine, McMaster University, Hamilton, Ontario, Canada

³Department of Psychiatry and Behavioural Neurosciences, McMaster University, Hamilton, Ontario, Canada

Corresponding author:

Gurmit Singh, Department of Pathology and Molecular Medicine, McMaster University, MDCL-2102, 1280 Main Street West, Hamilton, Ontario L8N 3Z5, Canada.

Email: singhg@mcmaster.ca



the fundamental mechanisms supporting the development of CIBP.

CIBP is a unique pain state that includes aspects of nociceptive, neuropathic, and inflammatory pain^{6,7} and is directly induced by many processes including pathological remodelling of the bone and nervous system and by secreted factors from cancer and host tissues, including substance P (SP).⁷⁻⁹ CIBP is characterized by neurochemical, cellular, and signalling features that are not uniformly shared across other pain states, including severe mechanical and thermal allodynia and hyperalgesia,¹⁰⁻¹⁶ central sensitization at the dorsal horn,^{12,14,15,17} peripheral sensitization of primary afferent C nociceptors,^{9,10,16,18} and cellular/neurochemical changes in the dorsal root ganglia (DRG) and dorsal horn of the spinal cord.^{8,17,19} Peripheral and central neurons are undeniably the structures that transmit the signals perceived as pain (see this excellent review by Woolf²⁰), and it is evident that ectopic activities of primary nociceptive sensory neurons contribute to peripheral sensitization and tumour-induced hyperalgesia of CIBP.¹⁶ However, no single study has characterized the primary nociceptor neuroelectrical changes that occur in bone cancer to connect these to the pain-related behaviours and the expression of SP in the same neurons—from the cutaneous receptive field to the DRG. This knowledge gap hinders progress in our understanding of the underlying cellular mechanisms of CIBP.

To address this gap, we have developed an immunocompetent rat model of CIBP using intrafemoral implantation of MAT-LyLu (MLL) murine prostate cancer cells that demonstrates mechanical hypersensitivity to tactile stimuli.¹¹ However, it remained unclear which functional subgroups of afferent neurons are involved in altering the nociceptive behaviour. Previous studies of nociceptors in CIBP examined DRG neurons *ex vivo* or applied *in vivo* extracellular recordings of DRG neurons that were only anatomically or partially functionally identified.^{10,16} To better elucidate the possible contributions of primary sensory neurons to CIBP, we performed intracellular *in vivo* electrophysiological recordings from DRG somata that remained functionally connected to their sensory receptors. Every neuron was characterized on the basis of several functional and morphological parameters, including the configuration of the action potential (AP), axonal conduction velocity (CV), activation of the sensory receptive field, and expression of SP. SP is a neuropeptide that is indicative of nociceptive neurons and is responsible for nociceptive transmission from the peripheral to the central nervous system.²¹ Following electrophysiological classification, the properties of DRG neurons from cancer rats were compared with those from control rats.

We report here that SP expressing nociceptive mechanosensitive neurons categorized into three

types of primary sensory fibres (C, A δ , and A β -fibres) show differences in excitability and functional properties concurrent with behavioural responses suggesting pain sensation and thus might play an essential role as a trigger of tactile hypersensitivity in CIBP.

Methods

Experimental rats and tumour induction

All experimental procedures conformed to the Guide to the Care and Use of Laboratory Animals, Volumes 1 and 2, of the Canadian Council on Animal Care, and all protocols were reviewed and approved by the McMaster University Animal Research Ethics Board. Male Copenhagen rats (Harlan Laboratories Inc., Indianapolis, IN) weighing 200–250 g were randomly assigned to groups and induced as a model of CIBP as described in our previous study.¹¹ Briefly, cancer rats were anaesthetised with inhaled isoflurane (1–5% in oxygen) and 5.0×10^6 MLL cells suspended in 0.1 mL phosphate buffer saline (PBS) were injected into the distal epiphysis of the femur by manual rotation of a 25 ga needle between the medial and lateral condyles. Sham injection (*control*) rats received an injection of 0.1 mL PBS only by the same procedures. Volume of injected material was minimized to ensure that it remained within the penetrated epiphysis, and surgical procedures were minimized to reduce the confounding influence of pain resulting from bone and soft tissue damage.

von Frey test of paw withdrawal threshold

In all cases, behavioural tests were performed immediately prior to anaesthesia for electrophysiological recordings to quantify the development of tactile hypersensitivity characteristic of CIBP. Rats were placed in a transparent Plexiglas box containing 0.5 cm diameter holes spaced 1.5 cm apart on the floor to allow full access to the paws.²²⁻²⁴ Animals were allowed to habituate to the box until cage exploration and major grooming activities had ceased.

von Frey filaments (Stoelting Co., Wood Dale, IL) were applied to the plantar surface of the ipsilateral hind paw to determine mechanical withdrawal thresholds using the up-down method of Dixon.²⁵ A von Frey filament was applied five times for 3–4 s each at 3-second intervals to a different spot on the plantar surface of the ipsilateral hind paw. Filaments were applied in ascending order of force until a clear withdrawal response was observed. When this occurred, the next lightest filament was reapplied, and the process continued until a 50% withdrawal response threshold was derived.²⁶ Brisk foot withdrawal in response to the

mechanical stimulus was interpreted as indicating mechanical hypersensitivity.

Intracellular recording in vivo

Details of acute intracellular electrophysiological recording techniques have been reported previously in animal models of neuropathic pain.^{27, 28} In brief, each rat was initially anesthetised with a mixture of ketamine, xylazine, and acepromazine delivered intraperitoneally. The right jugular vein was cannulated for intravenous infusion of drugs and the rat was fixed in a stereotaxic frame and the vertebral column rigidly clamped at the L2 and L6 vertebral levels. The right femur was fixed by a customized clamp onto the stereotaxic frame to minimize movement of the DRG during mechanical searching for receptive fields on the leg. The L4 DRG was selected for study, as it contains large numbers of hind leg afferent somata. A laminectomy was performed to expose the ipsilateral L4 DRG. The L4 dorsal root was sectioned close to the spinal cord and placed on a bipolar electrode (FHC, Bowdoinham, ME) used for stimulation. The exposed spinal cord and DRG were covered with warm paraffin oil at 37°C to prevent drying. Rectal temperature was maintained at 37°C using a temperature-controlled infrared heating lamp.

For recording, each rat was maintained at a surgical level of anaesthesia using sodium pentobarbital (20 mg/kg; Ceva Sante Animal, Libourne, France) and was mechanically ventilated via a tracheal cannula using a Harvard Ventilator (Model 683, Harvard Apparatus, Quebec, Canada). The ventilation parameters were adjusted so that end-tidal CO₂ concentration was maintained around 40–50 mmHg, as measured using a CapStar-100 End-Tidal CO₂ analyzer (CWE, Ardmore, PA). Immediately before the start of recording, an initial 1 mg/kg dose of pancuronium (Sandoz, Boucherville, QC, Canada) was given to eliminate muscle tone. The effects of pancuronium were allowed to wear off periodically to confirm a surgical level of anaesthesia; this was monitored by observing pupil diameter and response to noxious pinch of a forepaw. Supplementation of pentobarbital and pancuronium was administered at doses of 1/3 of the previous dose, approximately each hour via the jugular cannula.

Intracellular recordings from somata in the exposed DRG were made with borosilicate glass micropipettes (1.2 mm outside diameter, 0.68 mm inside diameter; Harvard Apparatus, Holliston MA). The electrodes were pulled using a Brown–Flaming pipette puller (model P-87; Sutter Instrument Co., Novato, CA). These electrodes were filled with 3 M KCl (DC resistance 50–70 MΩ). Signals were recorded with a Multiclamp 700B amplifier (Molecular Devices, Union City, CA) and digitized online via Digidata 1322 A interface

(Molecular Devices, Union City, CA) with pClamp 9.2 software (Molecular Devices, Union City, CA). The microelectrode was advanced using an EXFO IW-800 micromanipulator (EXFO, Montreal, QC, Canada) in 2 μm steps until an abrupt hyperpolarization of at least 40 mV appeared. Once a stable membrane potential had been confirmed, a single stimulus was applied to the dorsal root to provoke an AP. The protocol editor function in the pClamp 9.2 software was used to evoke a somatic AP by stimulation with a single rectangular intracellular depolarizing voltage pulse.

AP configuration

The first AP evoked by stimulation of the dorsal root and measured at the DRG soma in each neuron was used to compare the configuration between control and cancer rats. Criteria for acceptance of neurons in the subsequent analysis included a stable resting membrane potential more negative than –40 mV with a somatic spike evoked by dorsal root stimulation that was >40 mV. Variables in AP configuration included V_m, APA, APdB, APRT, APFT, AHPA, and AHP50.

Conduction velocity

The distance from the stimulation site (cathode) to the recording site (centre of the DRG) was measured at the end of the experiment to determine the conduction distance. This value was used to calculate the CV of the dorsal root axon associated with each neuron.

DRG neuron classification

Recorded neurons were classified as C, Aδ, or Aβ-fibres based on their AP configuration, CV, and their receptive properties defined by using handheld mechanical stimulators.^{27–31}

DRG neuron intracellular labelling

After physiological characterization by electrophysiological and functional properties, neurons that met the AP configuration criteria mentioned earlier were selected for subsequent histological identification by injection of neurobiotin (Vector Laboratories, Inc.) into the cell body. Recording microelectrodes were filled with 4% neurobiotin in 1 M KCl and this dye was ejected into the neuron by pulses of positive current (1 nA at 2 Hz, over 2 min).

Stimulation from different sites on sensory neurons

Different locations on the primary afferents were stimulated (Figure 1(b)) to determine excitability measured as

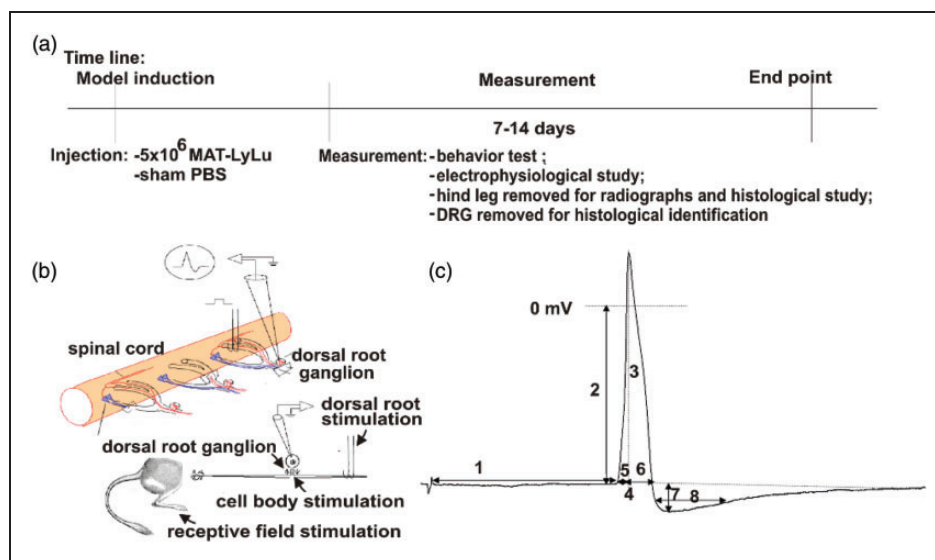


Figure 1. Model timeline, recording sites, and action potential parameters. (a) Illustrative timeline of procedures involving animals. Model induction of MLL cancer cell injected animals and control animals (PBS) occurred on experimental Day 0. Behavioural and electrophysiological procedures were performed between experimental Days 7 and 14. (b) Illustration of stimulation and recording sites for electrophysiological procedures. Recording occurred intracellularly for all neurons. Stimulation was performed at the receptive field by mechanical stimulation with von Frey filaments and also electrically at the dorsal root and the DRG soma. (c) A representative intracellular somatic action potential of a C-fibre neuron evoked by electrical stimulation of the dorsal root demonstrating the electrophysiological parameters measured, including: (1) conduction velocity; (2) resting membrane potential; (3) action potential amplitude; (4) action potential duration at base; (5) action potential rise time; (6) action potential fall time; (7) after hyperpolarization amplitude below V_m ; and (8) after hyperpolarization duration to 50% recovery.

MLL: MAT-LyLu rat prostate cancer cell line; PBS: phosphate buffer saline; DRG: dorsal root ganglia.

evoked APs in the soma, including stimulation of the soma by direct depolarizing current injection, electrical stimulation of the dorsal roots using bipolar stimulating electrodes, and mechanical activation of the peripheral receptive field.

Soma. To quantify soma excitability, the threshold of depolarizing current pulses injected into the soma was performed by applying pulses of 100 ms in increments of 0.05 nA through the recording electrode until an AP was elicited or until a maximum current of 4 nA was reached. The excitability of the soma was also evaluated by comparing the number of APs evoked by injecting defined current pulses to the DRG soma; three intracellular current injections of 100 ms each were delivered with 1, 1.5, and 2 nA.

Dorsal roots. Dorsal root excitability was measured by determining the chronaxie curve (threshold duration), which was defined by delivering the minimum current that would elicit an AP in the soma to the dorsal root using current pulse durations of 0.02, 0.1, 0.2, 0.4, and 0.6 ms. The stimulation pulse was delivered from an S940/910 stimulus adaptor/isolator (Dagan, Minneapolis, MN).

Peripheral receptive field. The response of DRG neurons to mechanical stimulation of cutaneous receptor fields was determined using calibrated von Frey filaments as described previously.^{27,32,33} Briefly, after functional classification of a neuron using the handheld mechanical stimulators, von Frey filaments were applied to the identified receptive field and the mechanical activation threshold of each neuron was expressed as the minimum force (g) necessary to evoke impulses on the most sensitive spot on the skin. The mechanical forces exerted with the calibrated von Frey filaments used in this study exerted forces equivalent to 0.008, 0.02, 0.04, 0.07, 0.16, 0.4, 0.6, 1.0, 1.4, 2.0, 4.0, 6.0, 8.0, 10, 15, 26, 60, 100, 180, and 300 grams; tip diameters ranged from 1.65 to 6.65 mm. Neurons that were not responsive to von Frey filaments were excluded from this part of the study.

Radiography and histology

After each electrophysiological recording experiment, both the ipsilateral hind legs of control and cancer rats were immediately dissected and shed of cutaneous tissue and muscle. Following dissection, all bone samples were immediately fixed in a 10% formalin solution in PBS for 72 h. High-resolution radiographs of dissected and fixed rat femurs were acquired with a Faxitron X-ray

MX-20 system (Faxitron, Lincolnshire, IL) on Kodak MIN-R 2000 Mammography Film (Kodak, Rochester, NY). Subsequently, the legs were decalcified in a 10% ethylenediaminetetraacetic acid in PBS (pH 7.4) solution for 4 weeks with the replacement of fresh solution every third day. Once decalcification was complete, samples were further processed and embedded in paraffin wax, then sectioned to 4 μm thickness using a microtome (Reichert-Jung 2040 Microtome; Reichert Inc., Depew, NY) and stained using H&E for light microscopy.

SP staining

L4 DRGs ipsilateral to the cancer-bearing limbs were surgically extracted, fixed in 4% paraformaldehyde, and cryostat sectioned at 25 μm thick transverse to the longitudinal axis. The sections were washed in PBS and incubated with blocking solution containing 10% normal goat serum at 25°C for 2 h. After overnight incubation with 1:500 rabbit anti-substance P (Millipore, AB1566, Billerica, MA) at 4°C, sections were washed in PBS and incubated with AlexaFluor 488 labelled goat anti-rabbit IgG (Invitrogen, Canada) diluted 1:2000 at 25°C for 2 h and viewed using a fluorescent microscope. For DRGs containing neurobiotin-injected neurons, these were also incubated with NeutrAvidin Texas Red 1:100 (Vector Laboratories) at 25°C for 2 h to reveal neurobiotin staining via light microscopy.

Statistical analysis

Data are presented as mean \pm the standard error of the mean. Response data were analyzed with Mann-Whitney U tests. $p < 0.05$ was considered to indicate a significant difference as shown in the graphs. GraphPad Prism software (GraphPad Software, Inc., La Jolla, CA) was used for all statistical analyses and graphing.

Results

Control rats ($n = 8$) and cancer rats ($n = 10$) were successfully completed with injections occurring on Day 0 and behavioural/electrophysiological testing completed between Days 7 and 14 (Figure 1(a)). Intracellular neuron recordings were made using the preparation shown in Figure 1(b). Intracellular somatic action potentials were evoked by electrical stimulation of the dorsal root in order to measure the following electrophysiological parameters (illustrated in Figure 1(c)): (a) conduction velocity (CV), (b) resting membrane potential (V_m), (c) AP duration at base (APdB), (d) AP rise time (APRT), (e) AP fall time (APFT), (f) AP amplitude (APA), (g) Afterhyperpolarization duration to 50%

recovery (AHP50), and (h) afterhyperpolarization amplitude (AHPA).

Rats with bone tumours show osteolysis and decreased mechanical threshold

Hematoxylin and eosin (H&E) stained sections of femurs from control rats demonstrate normal bone tissue including healthy marrow within the distal epiphysis and diaphysis and healthy mineralized bone (Figure 2(a), left). The ipsilateral distal femur sections from cancer rats show extensive tumour replacement of marrow within the epiphysis and eroded trabecular bone (Figure 2(a), right). Radiographs show that control rats exhibit normal bone density and structure (Figure 2(b), left). Evidence of atypical bone remodelling including significant osteolytic degradation is visible in the radiographs of cancer rats (Figure 2(b), right). Recorded immediately prior to electrophysiological experiments, cancer rats demonstrated behavioural evidence suggesting decreased threshold for mechanical stimulation in the ipsilateral limbs, while control rats did not (Figure 2(c)). Stimulation of the plantar surface of the hind paw evoked a withdrawal response in control rats, with filaments exerting pressures of 10–100 g. Filaments to which the control rats showed no withdrawal response, i.e., 4.0–8.0 g, evoked a clear withdrawal of the hind limb by cancer rats. Furthermore, the withdrawal was often exaggerated in amplitude and duration and accompanied by licking of the paw. Withdrawal thresholds were 12.20 ± 0.71 g in control ($n = 8$) and 6.80 ± 0.58 g in cancer rats ($n = 10$). These differences were statistically significant ($p < 0.0001$).

AP configuration is different between cancer and control rats

Intracellular electrophysiological recordings were made from a total of 78 functionally defined L4 DRG neurons (41 neurons in control and 37 neurons in cancer rats). In the control group, these included 16 C-, 9 A δ -, and 16 A β -fibre neurons, while in the cancer group, these included 15 C-, 8 A δ -, and 14 A β -fibre neurons. Neurons were included in these results based on the AP configuration criteria described in the Methods and the positive expression of SP. Functionally identified neurons that were isolated by identification of neurobiotin staining were then counterstained for SP immunoreactive material for morphological confirmation. Examples of C-, A δ -, and A β -fibre nociceptive neurons expressing positive staining for SP appear in Figure 3.

Following neuron type classification, the eight AP parameters of corresponding subclasses of neurons were compared between the control and cancer groups. All data are shown in the scatter plots of Figure 4,

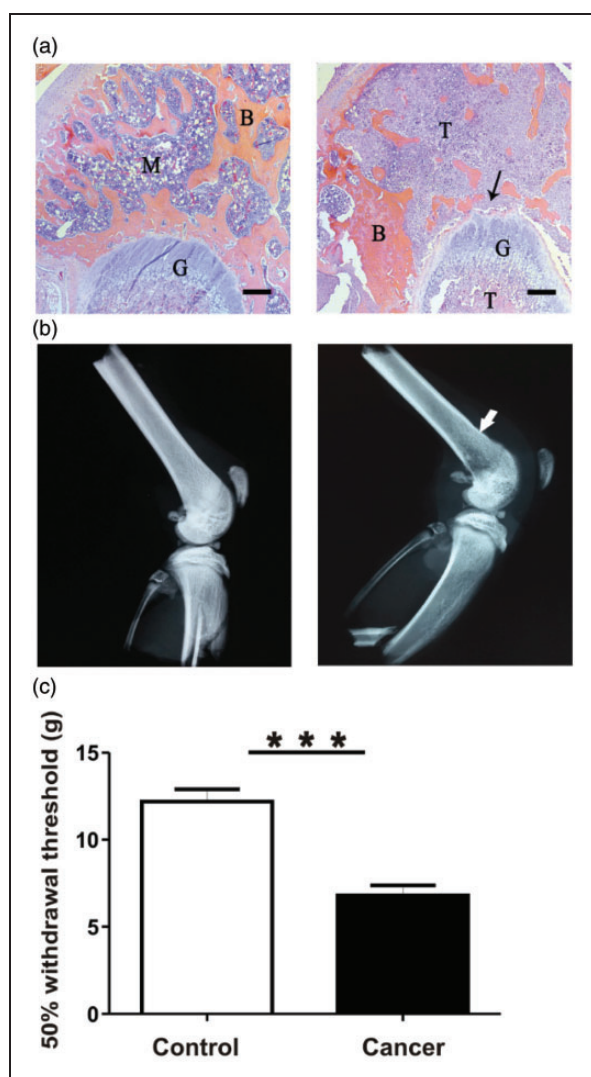


Figure 2. Model confirmation: structural and histological differences. (a) Representative H&E stained $4\mu\text{m}$ thick sections of the ipsilateral distal epiphysis of femurs from control (left) and cancer rats (right). Control bone appears healthy and free of indications of pathology induced by sham injections. In contrast, cancer bone features extensive invasion of cancer cells into areas of the bone marrow and mineralized bone; surfaces of trabecular bone appear ragged and eroded (indicated by arrow). B: mineralized bone; M: marrow; T: tumour cells; G: growth plate. Scale bar represents $300\mu\text{m}$. (b) Representative radiographs of ipsilateral hind limbs of control (left) and cancer rats (right). Control bone appears pathology-free, while cancer bone displays structural modifications and lytic lesions at the injection site in the distal femur epiphysis. All images were taken following fixation of samples from animals 7 to 14 days after model induction. (c) Comparison of 50% withdrawal thresholds between control and cancer groups. Withdrawal threshold to mechanical stimulation of the plantar surface of the ipsilateral hind paw with von Frey filaments was recorded immediately prior to the acute electrophysiological experiment in control ($n = 15$) and cancer ($n = 15$) animals. Data are shown as mean \pm SEM. *** $p < 0.001$. H&E: hematoxylin and eosin;

illustrating the distributions of the various parameters for individual neurons in each neuron type.

CV was not different

Comparison of the CV between control and cancer rats in each nociceptive neuron type did not show any significant differences. In C-fibre nociceptive neurons, CV was 0.56 ± 0.03 mm/ms in control versus 0.55 ± 0.03 mm/ms in cancer ($p = 0.851$; Figure 4(a), left). In $A\delta$ -fibre nociceptive neurons, CV was 4.46 ± 0.70 mm/ms in control versus 3.37 ± 0.71 mm/ms in cancer rats ($p = 0.290$; Figure 4(a), middle). In $A\beta$ -fibre nociceptive neurons, CV was 12.99 ± 0.67 mm/ms in control and 12.11 ± 0.93 mm/ms in cancer rats ($p = 0.441$; Figure 4(a), right).

Resting membrane potential more depolarized in C-fibres

C-fibre nociceptive neurons in cancer rats exhibited a significantly more depolarized Vm in cancer rats than in control rats (control, -64.94 ± 2.19 vs. cancer, -55.90 ± 2.48 , $p = 0.01$; Figure 4(b), left). Neither $A\delta$ -fibre nociceptive neurons nor $A\beta$ -fibre nociceptive neurons showed any significant differences in Vm between groups (control, -58.84 ± 3.28 vs. cancer, -51.87 ± 2.65 , $p = 0.13$; Figure 4(b), middle; control, -65.77 ± 2.16 vs. cancer, -62.22 ± 2.78 , $p = 0.311$; Figure 4(c), right).

APA was lower in C- and $A\delta$ -fibres

There were significant differences in APA between control and cancer rats in C- and $A\delta$ -fibre nociceptive neurons, but no differences between groups in $A\beta$ -fibre nociceptive neurons. In C-fibre nociceptive neurons, amplitude was reduced in cancer rats (control, 79.85 ± 2.31 mV vs. cancer, 66.57 ± 3.05 mV, $p = 0.002$; Figure 4(c), left). Similarly, for $A\delta$ -fibre nociceptive neurons, there was reduced amplitude in cancer rats (control, 79.39 ± 2.99 mV vs. cancer, 70.20 ± 3.00 mV, $p = 0.047$; Figure 4(c), middle). $A\beta$ -fibre nociceptive neurons showed no significant differences between groups (control, 77.32 ± 2.78 mV vs. cancer, 70.49 ± 2.94 mV, $p = 0.102$; Figure 4(c), right).

APdB lower for all neuron types

Neurons in cancer rats exhibited a lower APdB in control rats in all fibre types. In C-fibre nociceptive neurons, APdB was 3.09 ± 0.16 ms in control versus 2.25 ± 0.19 ms in cancer rats ($p = 0.002$; Figure 4(d), left). In $A\delta$ -fibre nociceptive neurons, APdB was 2.61 ± 0.28 ms in control versus 1.92 ± 0.11 ms in cancer rats ($p = 0.04$; Figure 4(d), middle). In $A\beta$ -fibre nociceptive neurons,

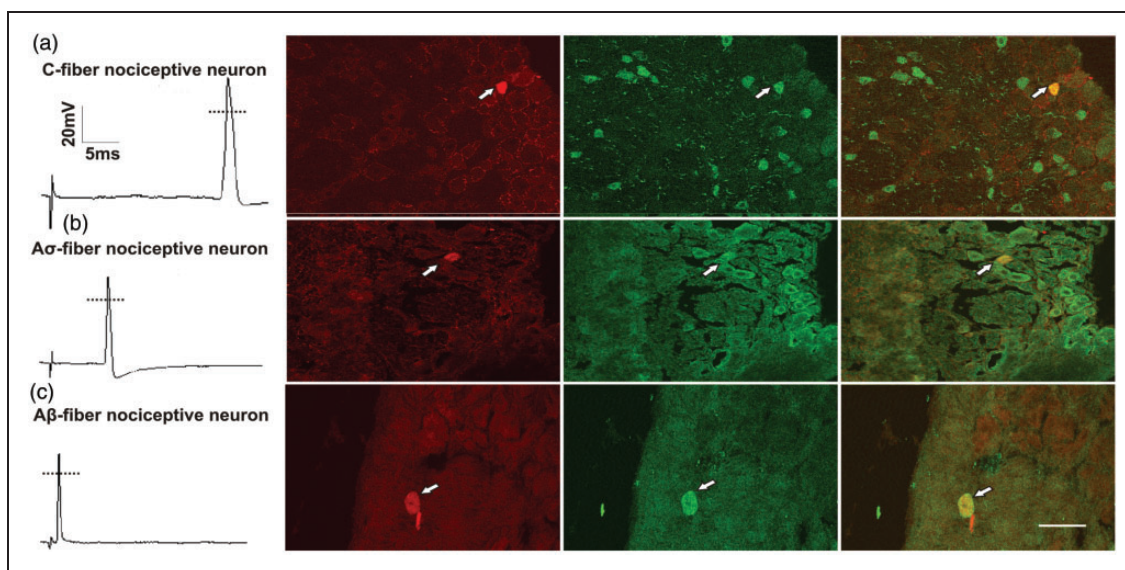


Figure 3. DRG classification and substance P colocalization. Examples of an evoked AP for each nociceptive neuron type (first column) and micrographs showing representative neurobiotin labelled DRG neurons in sections colabelled for SP. Each micrograph row consists of three images: left panel illustrates cells filled with neurobiotin in red (Texas Red); middle panel illustrates cells immunoreactive to SP in green (AlexaFluor 488); and right panel displays the merged images to show signal colocalization (yellow). Dye-labelled cells are indicated by arrowheads. Scale bar represents 50 μm . DRG: dorsal root ganglia; AP: action potential; SP: substance P.

APdB was 1.85 ± 0.09 ms in control versus 1.58 ± 0.06 ms in cancer rats ($p = 0.023$; Figure 4(d), right).

APRT shorter in C-fibre neurons

APRT did not differ between control and cancer rats in either A δ -fibre nociceptive neurons or A β -fibre nociceptive neurons. However, a shorter APRT was observed in C-fibre nociceptive neurons of cancer rats relative to control. In A δ -fibre nociceptive neurons, APRT was 0.98 ± 0.11 ms in control and 0.98 ± 0.06 ms in cancer rats ($p = 0.982$; Figure 4(e), left). In A β -fibre nociceptive neurons, APRT was 0.74 ± 0.07 ms in control and 0.70 ± 0.05 ms in cancer rats ($p = 0.585$; Figure 4(e), middle), whereas in C-fibre nociceptive neurons, APRT was 1.45 ± 0.07 ms in the control rats and 1.21 ± 0.08 ms in the cancer rats ($p = 0.034$; Figure 4(e), right).

APFT shorter for all neuron types

All nociceptive neurons exhibited significantly shorter APFT in the cancer group. C-fibre nociceptive neurons (control, 1.64 ± 0.13 ms vs. cancer, 0.99 ± 0.16 ms; $p = 0.003$; Figure 4(f), left), A δ -fibre nociceptive neurons (control, 1.63 ± 0.24 ms vs. cancer, 1.05 ± 0.18 ms; $p = 0.047$; Figure 4(f), middle), and A β -fibre nociceptive neurons (control, 1.10 ± 0.06 , vs. cancer, 0.89 ± 0.04 ; $p = 0.007$; Figure 4(f), right).

AHPA lower in C- and A δ -fibres

Differences in AHPA in cancer rats were observed in C-fibre and A δ -fibre nociceptive neurons, but no differences were observed between groups in A β -fibre nociceptive neurons. In C-fibre nociceptive neurons, there was a smaller amplitude in cancer rats (control, 9.51 ± 0.76 mV vs. cancer, 6.75 ± 0.98 mV, $p = 0.032$; Figure 4(g), left). Similarly, for A δ -fibre nociceptive neurons, there was a lower amplitude in cancer rats (control, 10.67 ± 1.29 mV vs. cancer, 6.29 ± 1.05 mV, $p = 0.021$; Figure 4(g), middle). In A β -fibre nociceptive neurons, there were no significant differences between groups (control, 8.66 ± 0.82 mV vs. cancer 7.89 ± 1.16 mV, $p = 0.589$; Figure 4(g), right).

AHP50 shorter in C- and A δ -fibres

Similar to AHPA, differences in AHP50 were observed between groups in C-fibre and A δ -fibre nociceptive neurons, but not in A β -fibre nociceptive neurons. In C-fibre nociceptive neurons, there were shorter durations in cancer rats (control, 12.51 ± 2.24 ms vs. cancer, 6.41 ± 1.36 ms, $p = 0.029$; Figure 4(h), left). Similarly, for A δ -fibre nociceptive neurons, there was reduced duration in cancer rats (control, 9.75 ± 1.59 ms vs. cancer, 4.81 ± 1.46 ms, $p = 0.039$; Figure 4(h), middle). In A β -fibre nociceptive neurons, there were no significant

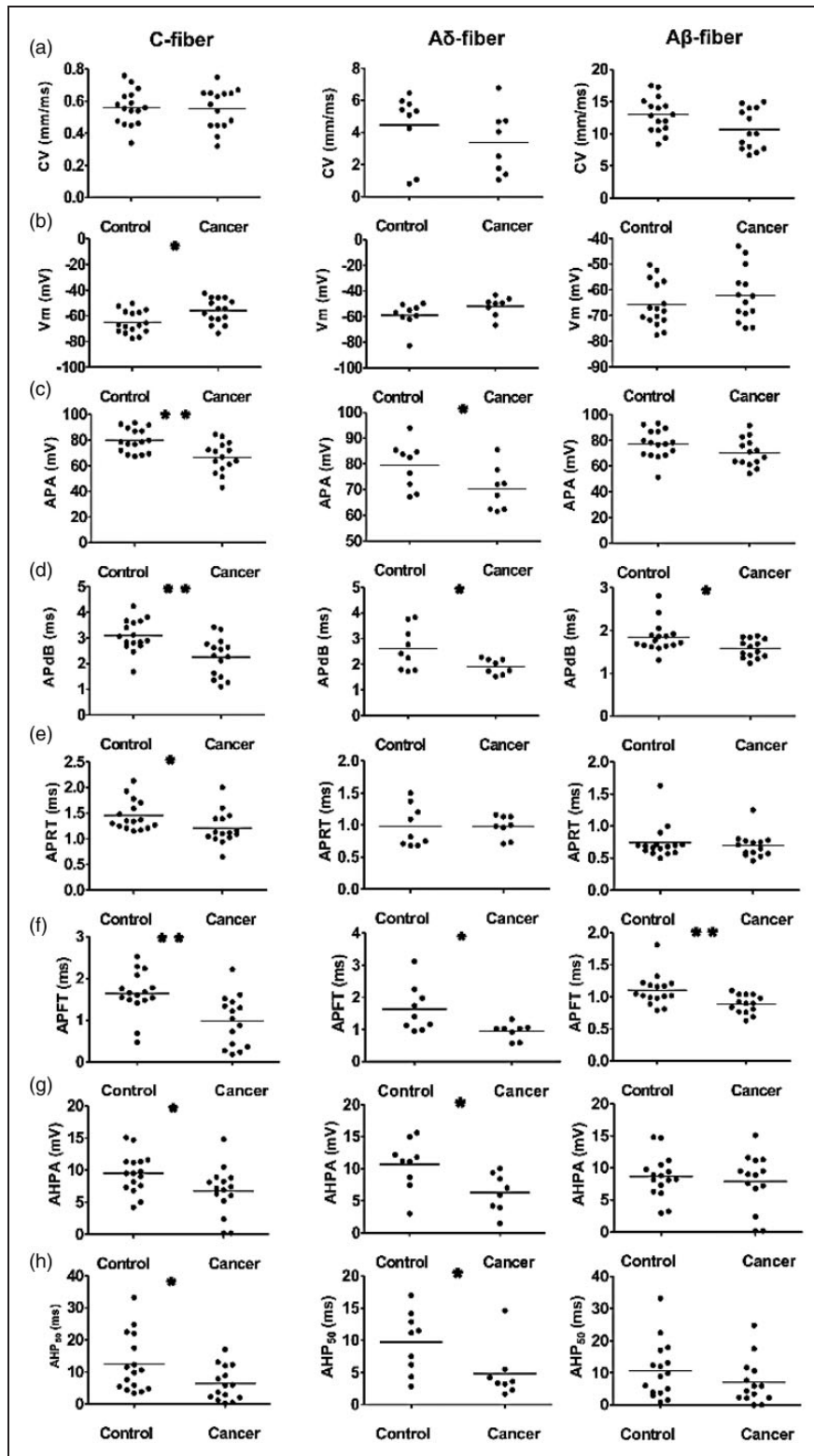


Figure 4. Action potential properties of DRG neurons in control and cancer rats. Scatter plots of properties of evoked APs in individual neurons. The median is superimposed as a horizontal line. Each column represents a specific neuron type: C-fiber nociceptive neurons (a), A δ -fiber nociceptive neurons (b), and A β -fiber nociceptive neurons (c). The recorded variable panels are in rows, as follows: (a) CV; (b) resting membrane potential (V_m); (c) APA; (d) AP_{dB}; (e) APRT; (f) APFT; (g) AHPA; and (h) after hyperpolarization duration to 50% recovery (AHP₅₀). Asterisks indicate differences between control and cancer rats: **p* < 0.05, ***p* < 0.01.

DRG: dorsal root ganglia; AP: action potential; APA: action potential amplitude; AP_{dB}: action potential duration at base; APRT: action potential rise time; APFT: action potential fall time; AHPA: after hyperpolarization amplitude below V_m; AHP₅₀: after hyperpolarization duration to 50% recovery; CV = conduction velocity.

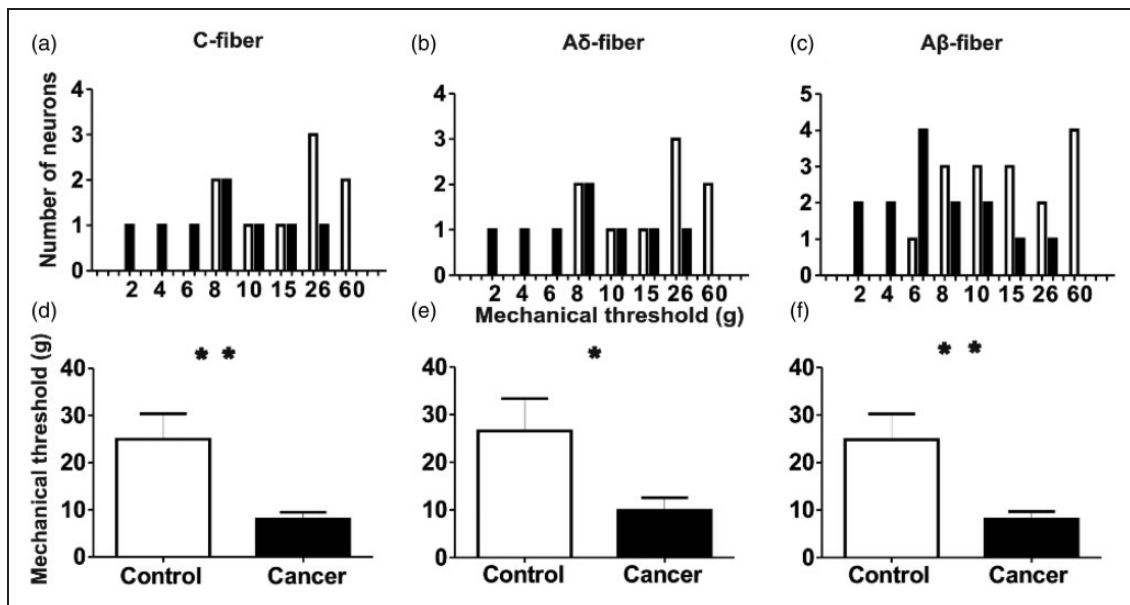


Figure 5. Comparison of the mechanical response threshold of DRG nociceptive neurons to application of von Frey filaments to the peripheral receptive fields of control and cancer rats. The upper row shows the distribution of the mechanical activation thresholds of the individual neurons. Columns indicate distribution of the number of neurons activated by each mechanical stimulus (in grams) in C- (a), A δ - (b) and A β -fibre (c) neurons in the cancer animals (filled bars) compared with the control animals (open bars). The lower row shows the mean mechanical response thresholds of neurons of each classification in control and cancer rats. * $p < 0.05$, ** $p < 0.01$. DRG: dorsal root ganglia.

differences between groups (control, 10.68 ± 2.18 ms vs. cancer, 7.03 ± 1.89 ms, $p = 0.224$; Figure 4(h), right).

DRG nociceptive neurons in cancer limbs have greater excitability

Lower response thresholds of DRG nociceptive neurons to mechanical stimulation of receptive field in cancer rats. The receptive field mechanical thresholds to nociception of DRG neurons were measured with von Frey filaments during electrophysiological recording. von Frey filaments were applied to the identified receptive field areas as a tactile stimulus and the minimum filament to elicit an AP in the soma was recorded. In cancer rats, all three types of nociceptive neurons required less forceful stimulation to elicit an AP than control rats (Figure 5). Figure 5(a) to (c) displays the distribution of the mechanical activation thresholds of individual neurons. The distribution is different for all three types of neurons in the cancer rats compared with the control rats. The mean mechanical threshold of the C-fibre nociceptive neurons in cancer rats is 7.93 ± 1.54 ($n = 15$), whereas control rats is 24.94 ± 5.42 ($n = 16$); ($p = 0.007$; Figure 5(d)). Thresholds of A δ -fibre nociceptive neurons were 26.56 ± 6.81 ($n = 9$) in control and 9.88 ± 2.69 ($n = 8$) in cancer rats ($p = 0.046$; Figure 5(e)). Thresholds of A β -fibre nociceptive neurons in control rats were

24.81 ± 5.44 ($n = 16$) and 8.07 ± 1.66 ($n = 14$) in cancer rats ($p = 0.009$ Figure 5(f)).

Attenuated soma excitability threshold and increased sensitivity to AP propagation of DRG nociceptive neurons in cancer rats. The current stimulation threshold required to induce an AP and the number of APs in response to intracellular depolarizing current pulse injection were recorded to determine whether there is a difference in soma excitability induced by cancer in the bone. Compared to control, all types of nociceptive neurons in cancer rats propagated an AP in response to lower threshold current injection of the soma (Figure 6(a) to (c)). The AP activation threshold of C-fibre nociceptive neurons was 2.91 ± 0.27 nA ($n = 7$) in control rats versus 1.54 ± 0.54 nA ($n = 5$) in cancer rats ($p = 0.037$; Figure 6(a)). The activation threshold of A δ -fibre nociceptive neurons was 2.95 ± 0.78 nA in control ($n = 4$) and 0.94 ± 0.26 nA in cancer ($n = 4$) rats ($p = 0.049$; Figure 6(a) and (b)). The activation threshold of A β -fibre nociceptive neurons was 2.46 ± 0.38 nA in control ($n = 9$) and 1.00 ± 0.28 nA in cancer rats ($n = 10$; $p = 0.006$; Figure 6(a) and (c)).

The responses to repetitive AP discharge were analyzed quantitatively by frequency-current analysis. All neurons in cancer rats demonstrated a trend towards more APs in response to intracellular current injection

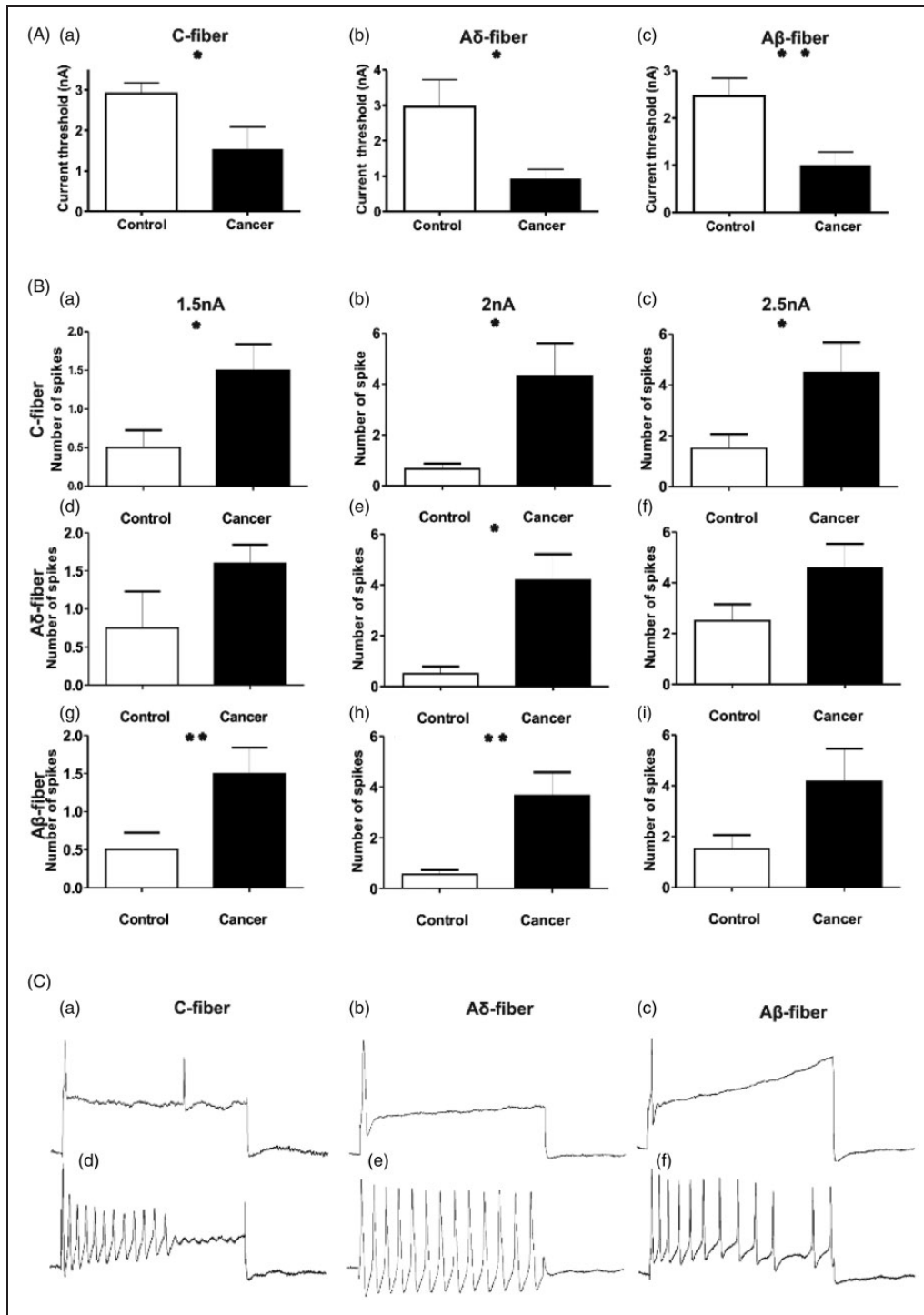


Figure 6. Comparison of the activation threshold of DRG nociceptive neurons in response to intracellular current injection, between control and cancer rats. (A) The current threshold is the minimum current required to evoke an AP by intracellular current injection to the soma of DRG neurons. Excitability of the DRG somata was significantly higher in cancer rats relative to control rats, as indicated by lower mean current activation threshold in all types of nociceptive fibres: C-fiber neurons (a), A δ -fiber neurons (B) and A β -fiber neurons (c). (b) A comparison the repetitive discharge characteristics of DRG cells produced by intracellular current injection at the soma. Columns indicate the number of APs evoked by intracellular injection of different magnitudes (Left = 1.5 nA, 100 ms. Middle = 2 nA, 100 ms. Right = 2.5 nA, 100 ms) of depolarizing current in C-fibres (a–c), A δ -fibres (d–f) and A β -fibres (g–i). Most neuron types in cancer rats produced a greater number of APs in response to depolarizing current than control rats. (C) Representative examples of raw recordings to demonstrate the greater number of APs evoked by intracellular current injection in cancer (d–f) than in control rats (a–c) in all neuron fibre types. APs in these examples were evoked by current pulses of 2 nA, 100 ms. * $p < 0.05$, ** $p < 0.01$. DRG = dorsal root ganglia; AP: action potential;

relative to control rats, although this trend was not always statistically significant in all neuron types at all stimulation currents. Figure 6(b) shows the number of APs in all nociceptive neuron fibre types elicited with three representative current strengths of 1.5, 2.0, and 2.5 nA, each at 100 ms injected to the soma.

In C-fibre nociceptive neurons (control, $n=6$; cancer, $n=6$), a 1.5 nA, 100 ms current injection elicited 0.50 ± 0.22 APs in control rats and 1.50 ± 0.341 in cancer rats ($p=0.034$; Figure 6(a) and (b)). With a 2.0 nA, 100 ms current injection, the number of APs in control rats was 0.67 ± 0.21 , whereas cancer rats exhibited 4.33 ± 1.28 ($p=0.0181$; Figure 6(b)). With a 2.5 nA, 100 ms current injection, the number of APs in control rats was 1.50 ± 0.56 , whereas in cancer rats, it was 4.50 ± 1.18 ($p=0.044$; Figure 6(b) and (c)).

In A δ -fibre nociceptive neurons (control $n=4$; cancer $n=5$), a 1.5 nA, 100 ms current injection elicited 0.75 ± 0.48 APs in control rats and 1.60 ± 0.25 in cancer rats ($p=0.135$; Figure 6(b) and (d)). With a 2.0 nA, 100 ms current injection, the number of APs in control rats was 0.50 ± 0.29 , whereas cancer rats exhibited 4.20 ± 1.02 ($p=0.017$; Figure 6(b) and (e)). With a 2.5 nA, 100 ms current injection, the number of APs in control rats was 2.50 ± 0.65 , whereas in cancer rats, it was 4.60 ± 0.93 ($p=0.122$; Figure 6(b) and (f)).

In A β -fibre nociceptive neurons (control $n=9$; cancer $n=9$), a 1.5 nA, 100 ms current injection elicited 0.33 ± 0.17 APs in control rats and 1.44 ± 0.24 in cancer rats ($p=0.002$; Figure 6(b) and (g)). With a 2.0 nA, 100 ms current injection, the number of APs in control rats was 0.56 ± 0.18 , whereas cancer rats exhibited 3.67 ± 0.91 ($p=0.004$; Figure 6(b) and (h)). With a 2.5 nA, 100 ms current injection, the number of APs in control rats was 2.00 ± 0.72 , whereas in cancer rats, it was 4.11 ± 1.02 ($p=0.111$; Figure 6(b) and (i)).

Figure 6(a) to (c) shows typical discharge patterns elicited in nociceptive neurons by 2.0 nA current pulses with a duration of 100 ms injected at the DRG soma. In response to current injection, nociceptive sensory neurons of all fibre types in control animals propagated 1–2 APs, while cancer rats propagated up to 12–13 APs with the same 2.0 nA current pulse injection.

Diminished dorsal root activation threshold and increased AP response of DRG nociceptive neurons in cancer rats

Dorsal root excitability was determined as the chronaxie curve (threshold duration), which was derived by determining the minimum current with pulse durations of 0.02, 0.1, 0.2, 0.4, and 0.6 ms applied to the dorsal root, that could evoke an AP at the corresponding neuronal soma (Figure 7(a)). All neuron types propagated APs at lower current intensities in cancer animals than

in control animals, although statistically significant differences were not observed over all tested current durations. In C-fibre nociceptive neurons, APs in cancer rats were evoked at a significantly lower current intensity threshold with 0.02 ms stimulation (0.98 ± 0.13 mA, $n=3$) than in control rats (1.63 ± 0.19 mA, $n=3$; $p=0.047$; Figure 7(a)). A δ -fibre nociceptive neurons also showed a significantly lower current intensity threshold to AP induction at 0.02 ms stimulation in cancer (0.87 ± 0.13 mA, $n=3$) than in control rats (1.50 ± 0.17 mA, $n=3$; $p=0.042$; Figure 7(a) and (b)). A β -fibre nociceptive neurons showed a significantly lower current intensity threshold to AP induction with 0.1 ms stimulation in cancer (0.27 ± 0.06 mA, $n=4$) rats than in control rats (0.57 ± 0.01 mA, $n=3$; $p=0.007$; Figure 7(a) and (c)).

Figure 7(a) to (e) shows typical discharge patterns elicited by 1 mA current pulses with a duration of 0.4 ms injected intracellularly at the dorsal root. In this figure, control rats exhibited 1 AP in response to current injection (a–c), whereas 2–5 APs were recorded in cancer rats in response to the same current pulse injection (d–e).

Discussion

Metastatic bone cancer is common and occurs with high incidence in patients with primary tumours of several types, including the breast, lung, and prostate.^{12,34} These tumours are frequently associated with severely debilitating outcomes such as pain, fractures, and hypercalcaemia. CIBP has been reported to be an unique and heterogeneous pain state driven by a combination of features of nociceptive, inflammatory, and neuropathic pain.⁶ Although assumed to be involved in the development of CIBP, the precise contribution of changes in peripheral sensory nociceptor functions to central pain perception had not yet been comprehensively defined. Our study addresses this knowledge gap by showing that CIBP-related behaviours correspond with increased excitability and differences in intrinsic membrane properties of three types of primary sensory neurons: C-, A δ -, and A β -fibres. With our unique combination of techniques, primary afferents in the DRG were classified functionally based on AP and morphological characteristics after being identified using mechanical stimulation of the receptive fields from the affected limb. Furthermore, these same neurons involved in the measured pain-related behaviours were also labelled intracellularly to aid in demonstrating SP expression, an important feature of nociceptive neurons.^{35–37}

Greater neuronal excitability in DRG neurons in cancer was revealed as a decreased threshold to AP activation by mechanical stimulus at the peripheral receptive field, a greater excitatory discharge response to injection of depolarizing current into the soma, and a greater

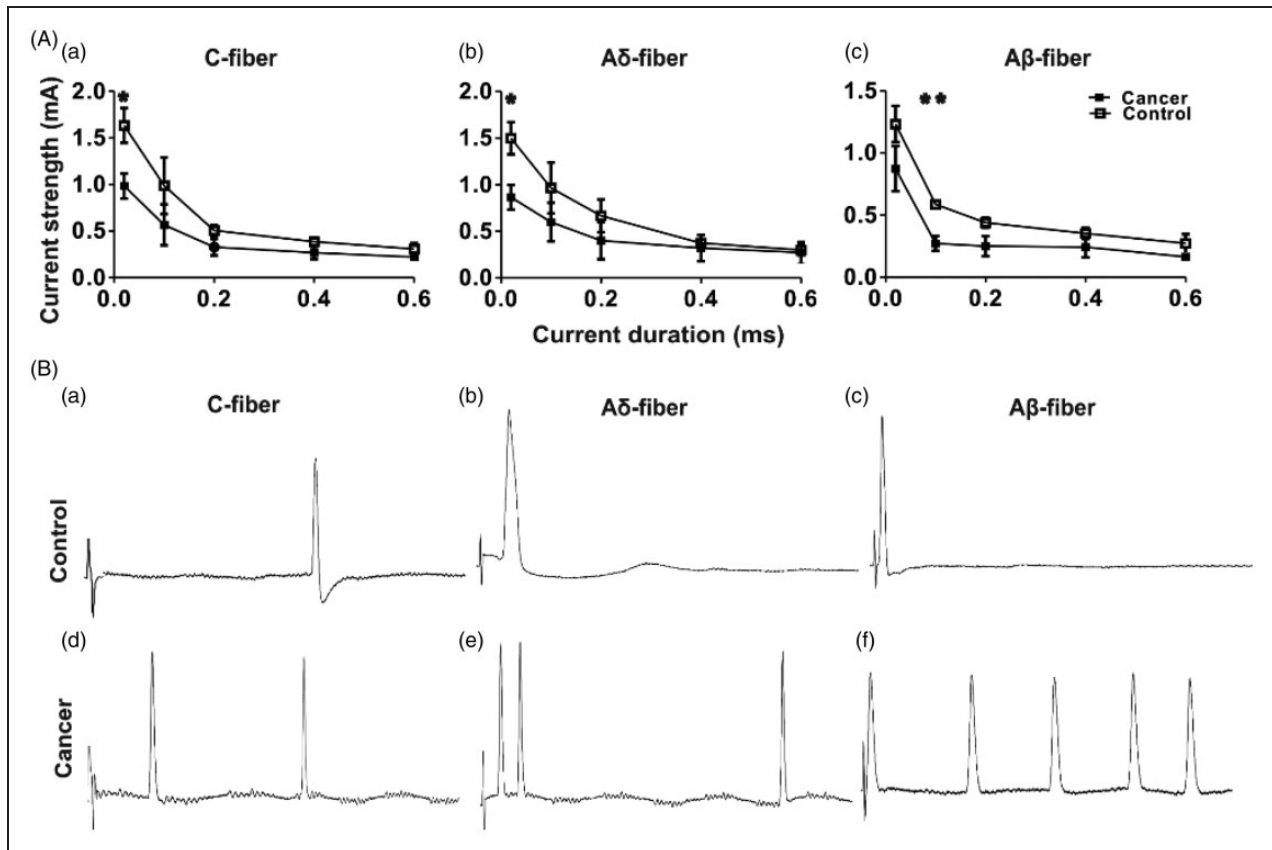


Figure 7. Comparison of current activation threshold of DRG nociceptive neurons in response to stimulation of the dorsal roots, between control and cancer rats. (A) Current activation threshold of DRG nociceptive neurons in response to stimulation of the dorsal roots. Current threshold was defined using the rheobase/chronaxie curve (threshold duration), which was determined as the minimum stimulus current to the dorsal root sufficient to evoke an AP with pulses of 0.02 ms, 0.1 ms, 0.2 ms, 0.4 ms, and 0.6 ms duration. C-fibre neurons (a), A δ -fibre neurons (b), and A β -fibre neurons (c) show a lower rheobase in cancer rats compared with controls. * $p < 0.05$, ** $p < 0.01$; (B) Representative recordings of the repetitive discharge characteristics of DRG neurons evoked by dorsal root stimulation by current pulses of 1 mA, 0.4 ms. DRG = dorsal root ganglia; AP: action potential.

response to electrical stimulation of the dorsal roots. Differences in intrinsic membrane properties of nociceptive DRG neurons between groups were also observed, including a depolarized resting membrane potential, a significant decrease in amplitude and duration of evoked APs, and a significantly lower in amplitude and duration of the AHPs in cancer rats. These functional differences in the cancer group may be due to membrane remodelling that has altered the intrinsic electrogenic properties of nociceptive neurons. Three ion channels, Na⁺, Ca²⁺, and K⁺, play major roles in determining the electrogenic properties of neurons. Alterations in expression, cellular localization, distribution, or the activation/kinetics of each of these ion channel types may manifest in the AP configuration differences that we have observed between cancer and control rats. For example, differences in expression and activation of both voltage-gated and Ca²⁺-activated K⁺ channels have been

reported as likely to contribute to alterations in the AHP.²⁹ Attenuated AP and AHP reduces inhibition of AP firing,^{16,38–40} thus the reduced AP and AHP duration and amplitude observed in nociceptors of cancer rats would be expected to increase the number of APs in response to stimuli, thus increasing the intrinsic excitability of those neurons. Although voltage-gated Na⁺ channels have been examined closely in rodent CIBP models, their involvement in sensitization of DRG neurons in the current model remains unclear. A significant downregulation of Na_v1.8 Na⁺ channel expression was found in a rat model of CIBP,⁴¹ although others observed that both Na_v1.8 and Na_v1.9 tetrodotoxin-resistant Na⁺ channels were significantly upregulated⁴² but only late in cancer progression. Further complicating this potential mechanism is a recent study that suggests that Na_v1.7 and Na_v1.8 channels appear not to be required for the development of CIBP.⁴³ Although a viable mechanism that

could lead our observed hyperexcitability in DRG neurons, the current study is not able to address this directly. Future experiments will be required to focus specifically on Na⁺ channel involvement in this phenomenon.

To our knowledge, this is the first study to perform *in vivo* intracellular electrophysiological recording of DRG neurons that remain connected to their receptive fields in an animal model of bone cancer pain. Several groups have investigated the parameters of central sensitization at the dorsal horn and reported different stimulation thresholds in the spinal cord in postsynaptic areas innervated by peripheral nociceptors in cancer.^{12,14,15} Others have also applied electrophysiological recording to peripheral sensory neurons in animal models of cancer pain and have suggested that peripheral sensitization plays a role in CIBP.^{10,16} A point of differentiation between their work and the current study is that our data were derived from intracellular *in vivo* recordings from DRG sensory neurons that remained fully connected to their receptive fields, and we evaluated differences in excitability at the soma, axon and the peripheral mechanical receptors. All included neurons in our study were classified based on the characteristics of mechanical stimulation threshold, CV, AP configuration, and SP expression.

Conclusions

Defining the physiological contributions of peripheral sensory neurons to CIBP is critical for the development of novel mechanism-based interventions for this frequent outcome of bone metastasis. As such, the purpose of the present study was to examine the electrophysiological properties and mechanical thresholds of different types of nociceptive neurons in an animal model of CIBP. We report that the animals with prostate cancer bone tumours have reduced mechanical thresholds in the tumour-bearing limb concurrent with enhanced primary nociceptor excitability and multiple differences in the intrinsic membrane properties of SP-expressing DRG neurons. These observations suggest that peripheral sensitization of nociceptive neurons may contribute to CIBP. Based on these results, we now have a more comprehensive understanding of this unique pain state at the cellular level that may allow for further development in mechanism-based treatments for CIBP.

Authors' contributions

YFZ and RU performed the experiments. YFZ, RU, and NZ performed the histological analysis. YZF and ES analyzed the data. YFZ, ES, and GS drafted the manuscript. ES, JH, JLH, and GS provided expertise and advice for the conception and design of the project and on the experimental techniques. All authors edited and approved the final version of the manuscript.

Declaration of Conflicting Interests

The author(s) declared no potential conflicts of interest with respect to the research, authorship, and/or publication of this article.

Funding

The author(s) disclosed receipt of the following financial support for the research, authorship, and/or publication of this article: This study was supported by the Canadian Institutes of Health Research (GS) and a post-doctoral fellowship (YFZ) from the Michael G. DeGroot Institute for Pain Research and Care.

References

1. Cleeland CS, Bennett GJ, Dantzer R, et al. Are the symptoms of cancer and cancer treatment due to a shared biologic mechanism? A cytokine-immunologic model of cancer symptoms. *Cancer* 2003; 97: 2919–2925.
2. Krishnasamy M. Fatigue in advanced cancer—meaning before measurement? *Int J Nurs Stud* 2000; 37: 401–414.
3. Mercadante S. Malignant bone pain: pathophysiology and treatment. *Pain* 1997; 69: 1–18.
4. Nijs J, Van de Velde B and De Meirleir K. Pain in patients with chronic fatigue syndrome: does nitric oxide trigger central sensitisation? *Med Hypotheses* 2005; 64: 558–562.
5. Sabino MA, Ghilardi JR, Jongen JL, et al. Simultaneous reduction in cancer pain, bone destruction, and tumor growth by selective inhibition of cyclooxygenase-2. *Cancer Res* 2002; 62: 7343–7349.
6. Colvin L and Fallon M. Challenges in cancer pain management—bone pain. *Eur J Cancer* 2008; 44: 1083–1090.
7. Clohisy DR and Mantyh PW. Bone cancer pain. *Cancer* 2003; 97: 866–873.
8. Schwei MJ, Honore P, Rogers SD, et al. Neurochemical and cellular reorganization of the spinal cord in a murine model of bone cancer pain. *J Neurosci* 1999; 19: 10886–10897.
9. Zhao J, Pan HL, Li TT, et al. The sensitization of peripheral C-fibers to lysophosphatidic acid in bone cancer pain. *Life Sci* 2010; 87: 120–125.
10. Cain DM, Wacnik PW, Turner M, et al. Functional interactions between tumor and peripheral nerve: changes in excitability and morphology of primary afferent fibers in a murine model of cancer pain. *J Neurosci* 2001; 21: 9367–9376.
11. De Ciantis PD, Yashpal K, Henry J, et al. Characterization of a rat model of metastatic prostate cancer bone pain. *J Pain Res* 2010; 3: 213–221.
12. Khasabov SG, Hamamoto DT, Harding-Rose C, et al. Tumor-evoked hyperalgesia and sensitization of nociceptive dorsal horn neurons in a murine model of cancer pain. *Brain Res* 2007; 1180: 7–19.
13. Ungard RG, Seidlitz EP and Singh G. Inhibition of breast cancer-cell glutamate release with sulfasalazine limits cancer-induced bone pain. *Pain* 2014; 155: 28–36.
14. Urch CE, Donovan-Rodriguez T and Dickenson AH. Alterations in dorsal horn neurones in a rat model of cancer-induced bone pain. *Pain* 2003; 106: 347–356.

15. Yanagisawa Y, Furue H, Kawamata T, et al. Bone cancer induces a unique central sensitization through synaptic changes in a wide area of the spinal cord. *Mol Pain* 2010; 6: 38.
16. Zheng Q, Fang D, Cai J, et al. Enhanced excitability of small dorsal root ganglion neurons in rats with bone cancer pain. *Mol Pain* 2012; 8: 24.
17. Donovan-Rodriguez T, Dickenson AH and Urch CE. Superficial dorsal horn neuronal responses and the emergence of behavioural hyperalgesia in a rat model of cancer-induced bone pain. *Neurosci Lett* 2004; 360: 29–32.
18. Hamamoto DT, Khasabov SG, Cain DM, et al. Tumor-evoked sensitization of C nociceptors: a role for endothelin. *J Neurophysiol* 2008; 100: 2300–2311.
19. Peters CM, Ghilardi JR, Keyser CP, et al. Tumor-induced injury of primary afferent sensory nerve fibers in bone cancer pain. *Exp Neurol* 2005; 193: 85–100.
20. Woolf CJ. Pain: moving from symptom control toward mechanism-specific pharmacologic management. *Ann Intern Med* 2004; 140: 441–451.
21. Henry JL. Effects of substance P on functionally identified units in cat spinal cord. *Brain Res* 1976; 114: 439–451.
22. Pitcher GM, Ritchie J and Henry JL. Nerve constriction in the rat: model of neuropathic, surgical and central pain. *Pain* 1999; 83: 37–46.
23. Pitcher GM and Henry JL. Second phase of formalin-induced excitation of spinal dorsal horn neurons in spinalized rats is reversed by sciatic nerve block. *Eur J Neurosci* 2002; 15: 1509–1515.
24. Pitcher GM and Henry JL. Nociceptive response to innocuous mechanical stimulation is mediated via myelinated afferents and NK-1 receptor activation in a rat model of neuropathic pain. *Exp Neurol* 2004; 186: 173–197.
25. Dixon WJ. Efficient analysis of experimental observations. *Annu Rev Pharmacol Toxicol* 1980; 20: 441–462.
26. Chaplan SR, Bach FW, Pogrel JW, et al. Quantitative assessment of tactile allodynia in the rat paw. *J Neurosci Methods* 1994; 53: 55–63.
27. Zhu YF and Henry JL. Excitability of A-beta sensory neurons is altered in an animal model of peripheral neuropathy. *BMC Neurosci* 2012; 13: 15.
28. Zhu YF, Wu Q and Henry JL. Changes in functional properties of A-type but not C-type sensory neurons in vivo in a rat model of peripheral neuropathy. *J Pain Res* 2012; 5: 175–192.
29. Djouhri L, Bleazard L and Lawson SN. Association of somatic action potential shape with sensory receptive properties in guinea-pig dorsal root ganglion neurones. *J Physiol* 1998; 513(Pt 3): 857–872.
30. Lawson SN, Crepps BA and Perl ER. Relationship of substance P to afferent characteristics of dorsal root ganglion neurones in guinea-pig. *J Physiol* 1997; 505(Pt 1): 177–191.
31. Wu Q and Henry JL. Changes in A-beta non-nociceptive primary sensory neurons in a rat model of osteoarthritis pain. *Mol Pain* 2010; 6: 37.
32. Leem JW, Willis WD and Chung JM. Cutaneous sensory receptors in the rat foot. *J Neurophysiol* 1993; 69: 1684–1699.
33. Shim B, Kim DW, Kim BH, et al. Mechanical and heat sensitization of cutaneous nociceptors in rats with experimental peripheral neuropathy. *Neuroscience* 2005; 132: 193–201.
34. Coleman RE. Clinical features of metastatic bone disease and risk of skeletal morbidity. *Clin Cancer Res* 2006; 12: 6243s–6249s.
35. Henry JL. Naloxone fails to block substance P-induced excitation of spinal nociceptive units. *Brain Res Bull* 1983; 10: 727–730.
36. Yasphal K, Wright DM and Henry JL. Substance P reduces tail-flick latency: implications for chronic pain syndromes. *Pain* 1982; 14: 155–167.
37. De Koninck Y and Henry JL. Substance P-mediated slow excitatory postsynaptic potential elicited in dorsal horn neurons in vivo by noxious stimulation. *Proc Natl Acad Sci USA* 1991; 88: 11344–11348.
38. Gurtu S and Smith PA. Electrophysiological characteristics of hamster dorsal root ganglion cells and their response to axotomy. *J Neurophysiol* 1988; 59: 408–423.
39. Sah P and Faber ES. Channels underlying neuronal calcium-activated potassium currents. *Prog Neurobiol* 2002; 66: 345–353.
40. Yan J, Li JC, Xie ML, et al. Short-term sleep deprivation increases intrinsic excitability of prefrontal cortical neurons. *Brain Res* 2011; 1401: 52–58.
41. Miao XR, Gao XF, Wu JX, et al. Bilateral downregulation of Nav1.8 in dorsal root ganglia of rats with bone cancer pain induced by inoculation with Walker 256 breast tumor cells. *BMC Cancer* 2010; 10: 216.
42. Qiu F, Jiang Y, Zhang H, et al. Increased expression of tetrodotoxin-resistant sodium channels Nav1.8 and Nav1.9 within dorsal root ganglia in a rat model of bone cancer pain. *Neurosci Lett* 2012; 512: 61–66.
43. Minett MS, Falk S, Santana-Varela S, et al. Pain without nociceptors? Nav1.7-independent pain mechanisms. *Cell Rep* 2014; 6: 301–312.